Applied Catalysis B: Environmental 89 (2009) 613–619

Contents lists available at ScienceDirect

Applied Catalysis B: Environmental

journal homepage: www.elsevier.com/locate/apcatb

Efficient gas phase photodecomposition of acetone by Ru-doped Titania

Vendula Houšková *, Václav Štengl, Snejana Bakardjieva, Nataliya Murafa, Václav Tyrpekl

Institute of Inorganic Chemistry, Academic of Sciences of the Czech Republic, Husinec-Rez 250 68, Czech Republic

ARTICLE INFO

Article history:
Received 8 November 2008
Received in revised form 22 January 2009
Accepted 24 January 2009
Available online 3 February 2009

Keywords:
TiO_2
Doped
RuO_2
Urea
Photocatalytic activity

ABSTRACT

Nanocrystalline titania particles doped with ruthenium oxide have been prepared by homogenous hydrolysis of $TiOSO_4$ in aqueous solutions in the presence of urea. The synthesized particles were characterized by X-ray diffraction (XRD), Scanning Electron Microscopy (SEM), High Resolution Transmission Electron Microscopy (HRTEM), Selected Area Electron Diffraction (SAED) and surface area (BET) and porosity determination (BJH). The photocatalytic activity of Ru-doped titania samples was determined in the gas phase by decomposition of acetone during irradiation at 365 nm and 400 nm. The Ru-doped titania samples demonstrated enhanced photocatalytic activity under visible light. Ruthenium oxide causes the anatase to rutile transformation to occur at lower temperatures and decreasing of band-gap energy of Ru-doped samples.

1. Introduction

Photocatalytic degradation processes have been widely applied as techniques for the destruction of organic pollutants in wastewater and effluents. TiO_2 is widely used for photocatalytic air and water purification and many other purposes based on photocatalytic oxidation and decomposition of organic pollutants [1–4]. The material can be also used for solar energy storage and conversion [5], organic syntheses [6], etc. Titanium dioxide is one of the most popular and promising materials for these purposes, because of its stability, commercial availability and ecological safety. According to the literature [7–9], the photocatalytic activity of suspended TiO_2 in solution strongly depends on its physical properties (e.g., crystal structure, surface area, surface hydroxyls, and particle size).

In order to enhance its activity as a catalyst, much effort has been expended attempting to modify TiO_2 by doping with Ru, S, Te, Si, Ag, P and other materials [10–14]. Ohno et al. [15] have reported on Ruthenium-doped titania and its photocatalytic activity under visible light. Ru-based oxides such as Ru–Zr, Ru–Ti, Ru–Ta, and Ru–Sn binary oxides, have been widely used as the dimensionally stable anodes (DSA®) for oxygen and chlorine evolution reactions [16,17].

There has also been considerable interest in using RuO_2 electrodes for hydrogen evolution [18,19], and exploratory work on the use of RuO_2-based electrodes for the oxidation (destruction) of organic waste [20] and as high energy and power density capacitors has been presented [21].

Homogeneous hydrolysis with urea as a precipitating agent can be used for preparation of oxo-compounds, such as metal oxides and hydroxides or precursors of base mixed oxo-hydroxides. The urea method is based on the thermal decomposition of urea at temperatures >60 °C [22,23].

In this contribution, a Ru doped titania was prepared by homogeneous hydrolysis of ruthenium chloride, titanium oxosulphate ($TiOSO_4$) and urea at 100 °C and later controlled annealing in an oxygen atmosphere. The photocatalytic activity of the Ru-doped TiO_2 composites was tested using photodegradation of acetone in the gaseous phase (λ = 365 nm; 400 nm).

2. Experimental

2.1. Synthesis of Ru-doped titania

All chemicals used, ruthenium chloride ($RuCl_3$), titanium oxosulphate ($TiOSO_4$) and urea ($(NH_2)_2CO$), were of analytical grade and were supplied by Fluka and Sigma–Aldrich Ltd. $TiOSO_4$ (100 g) and 1 g (0.75; 0.5; 0.25; 0.1; 0.05; 0.01 or 0.005 g) of $RuCl_3$ were dissolved in 4L of distilled water and 300 g of urea was added. The reaction mixture was adjusted to pH 2 with sulfuric acid and heated at 100 °C under stirring for 8 hours. The resulting titania powders were washed with distilled water, decanted, filtered off and dried at 105 °C in a furnace. After annealing at 600 °C in an oxygen atmosphere for 2 hours the synthesis of the Ru-doped titania powders denoted as TiRu2_600, TiRu3_600, TiRu4_600, TiRu5_600, TiRu6_600, TiRu7_600 and TiRu8_600 was complete. For characteristics and nomenclature (see Table 2).

* Corresponding author. Tel.: +420 2 6617 3144; fax: +420 2 2094 1502.
E-mail address: houskova@iic.cas.cz (V. Houšková).

0926-3373/$ – see front matter © 2009 Elsevier B.V. All rights reserved.
doi:10.1016/j.apcatb.2009.01.023

2.2. Characterization methods

X-ray diffraction (XRD) patterns were obtained with a Siemens D5005 instrument using Cu Kα radiation (40 kV, 30 mA) and a diffracted beam monochromator. Qualitative analysis was performed with the DiffracPlus Eva Application (Bruker AXS) using the JCPDS PDF-2 database [24]. For quantitative phase analysis, mean coherence length analysis, and structural refinement, Rietveld analysis with DiffracPlus Topas (Bruker ASX) and structural models from the ICSD database were used [25]. Sample TiRu_1 was studied by in-situ heating in air on a PANalytical X'Pert PRO diffractometer using Co K radiation (40 kV, 30 mA) and a multichannel detector X'Celerator with an anti-scatter shield, equipped with a high temperature chamber (HTK 16, Anton Paar, Graz, Austria). The measurements started at room temperature and finished at 1000 °C.

The surface areas of samples were determined from nitrogen adsorption–desorption isotherms at liquid nitrogen temperature using a Coulter SA3100 instrument with outgas 15 min at 120 °C. The Brunauer–Emmett–Teller (BET) method was used for surface area calculation [26], the pore size distribution (pore diameter and pore volume of the samples) was determined by the Barrett–Joyner–Halenda (BJH) method [27].

Scanning electron microscopy (SEM) studies were performed using a Philips XL30 CP microscope equipped with energy-dispersive X-ray (EDX), Robinson, SE and BSE detectors. The sample was placed on an adhesive C slice and coated with 10 nm thick layer of Au–Pd alloy.

Transmission electron micrographs (TEM and HRTEM) were obtained using two instruments, namely a Philips EM 201 operated at 80 kV and a JEOL JEM 3010 operated at 300 kV (LaB6 cathode). A copper grid coated with a holey carbon support film was used to prepare samples for TEM observation. The powdered sample was dispersed in ethanol and the suspension treated in an ultrasonic bath for 10 min.

Diffuse reflectance UV/VIS spectra for the evaluation of photophysical properties were recorded in the diffuse reflectance mode (R) in the wavelength range of 200–800 nm and transformed to absorption spectra through the Kubelka–Munk function [28]. A PerkinElmer Lambda 35 spectrometer equipped with a Labsphere RSAPE-20 integration sphere with $BaSO_4$ as a standard was used. The band gap was obtained from a plot of the modified Kubelka–Munk function versus the energy of exciting light by converting the scanning wavelength (λ) into photon energies (E_{bg}).

DTA–TG–MS measurements were carried out using a simultaneous Netzsch Instrument STA 409 coupled to Quadrupol Mass Spectrometer Balzers QMS-420 under dynamic conditions in the air (flow rate 75 mL min^{-1}). The samples were heated at the rate of 10 K min^{-1}.

Infrared spectra were recorded using a Thermo-Nicolet Nexus 670 FT-IR spectrometer approximately in the ranges 4000–500 cm^{-1} and 500–50 cm^{-1}, respectively, with a single-reflection horizontal accessory on a Si crystal. The samples were prepared in the form of pellets in KBr at ambient conditions and measured in the transmission mode.

From the titania samples were prepared coatings with HEMA (Hydroxy Ethyl Methacrylate) coated onto glass substrate of 10 cm × 15 cm size. The sample (1 g) was firstly well dispersed in ethanol and then HEMA was added. As-prepared mixture was applied onto glass substrate by using film applicator of pre-defined thickness. Photocatalytic activity of as-prepared coatings was determined in stainless steel photoreactor (constructed in our lab.) at wavelengths of 365 and 400 nm by decomposition of acetone (1 ml) in the gaseous state. The percentage concentrations of

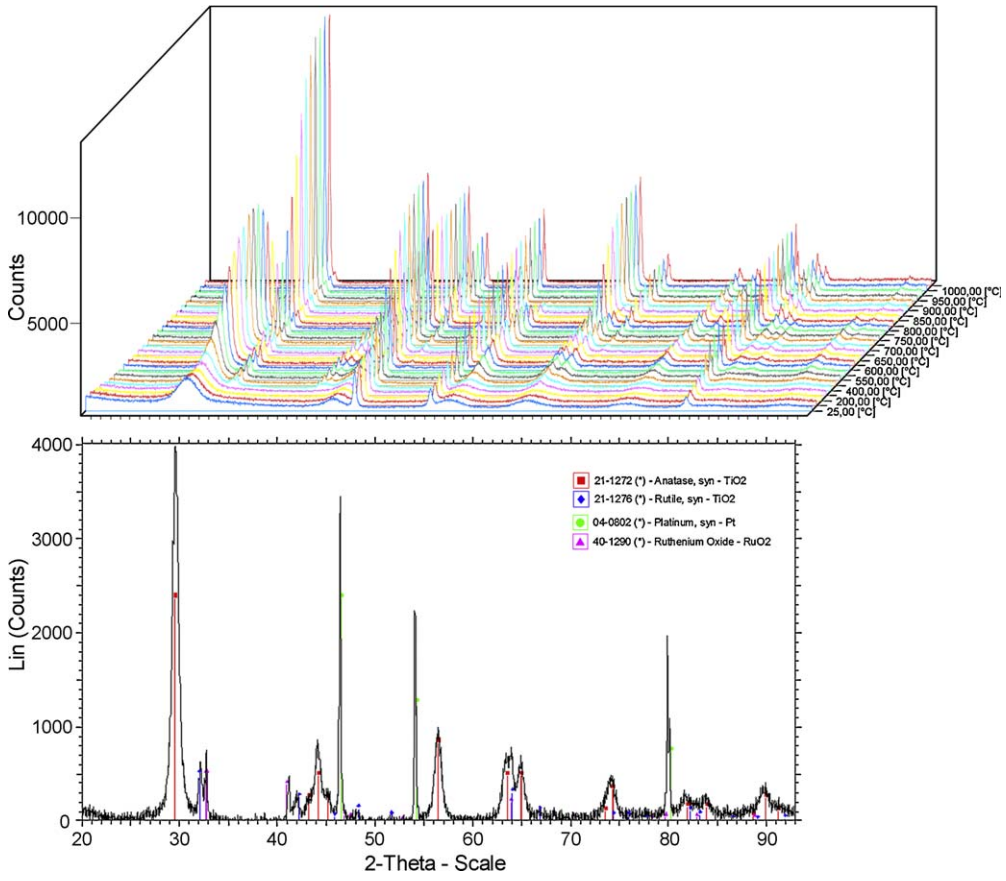

Fig. 1. XRD pattern of sample TiRu1 as a function of temperature (25–1000 °C).

Table 1
Crystallite sizes of anatase, rutile and RuO_2 phases in sample TiRu1 (determined by XRD).

Heat. temperature [°C]	Anatase crystallite size [nm]	Rutile crystallite size [nm]	RuO_2 crystallite size [nm]
1000	46.6	104	82.5
950	39.4	102.8	51.7
900	40.5	96.5	57.5
850	42.6	88.7	63.7
800	55.7	73.9	62.1
750	45.1	57.8	57.2
700	37.1	44.5	53.9
650	28.4	37.1	53.2
600	20.9	37.2	55.4
550	11.7	31.4	53.1
500	8.4	28.4	50.1
400	6.6	27	50
300	5.2	–	50
200	4.6	–	–
100	4.5	–	–
25	4.5	–	–

acetone and carbon dioxide were measured with a gas analyser based on infra-red detectors from Aseko Ltd., Czech Republic.

3. Results and discussion

3.1. X-ray diffraction (XRD)

The high temperature XRD diffractogram of sample TiRu1 (sample containing 3.83 mol.‰ ruthenium) is shown in Fig. 1. It is obvious that the anatase phase is present in the temperature range from 25 to 1000 °C. Ruthenium, analogous to the Fe, Th, Cu, Pd and other dopants, can assist the phase transformation at lower temperatures thanks to so-called strong-metal-support-interaction [29,30]. The transition from anatase to rutile modification takes place at ca. 400 °C unlike undoped TiO_2 which shows the anatase–rutile transition at 800 °C [31]. The absence of peaks from the ruthenium oxide phase may be attributed to their ultra fine dispersion on TiO_2 particles as very small clusters, or due to the very low dopant content.

Fig. 2 shows percentage content of each phase (anatase, rutile, RuO_2) as a function of the heating temperature of sample TiRu1 (model sample). Up to 600 °C the crystallinity of RuO_2 increases while at temperatures >600 °C, RuO_2 decreases because of the inclusion of Ru ions in the TiO_2 lattice [15]. This is possibly due to the comparable lattice parameters of RuO_2 and rutile. Table 1 shows average particle diameters of TiRu1 sample calculated from XRD peak broadening. Clearly, the particle sizes of anatase and rutile phases increase with increasing temperature. Crystallite sizes of samples annealed at 600 °C are shown in Table 2. From this it is clear that the content of RuO_2 has an influence on the particle size of anatase, which decreases with increasing amounts of RuO_2.

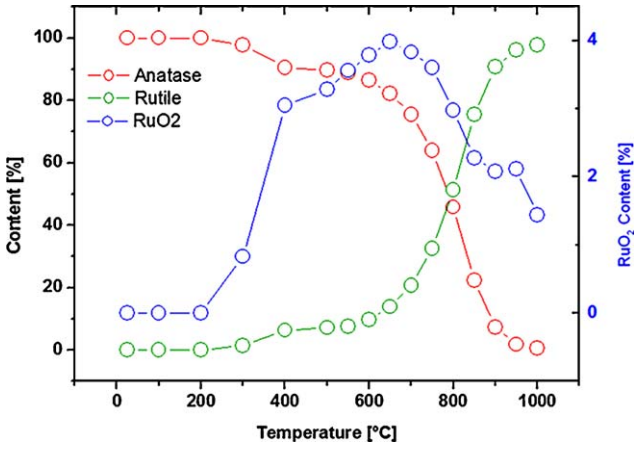

Fig. 2. Dependence of crystal phase evolution of TiRu1 on temperature.

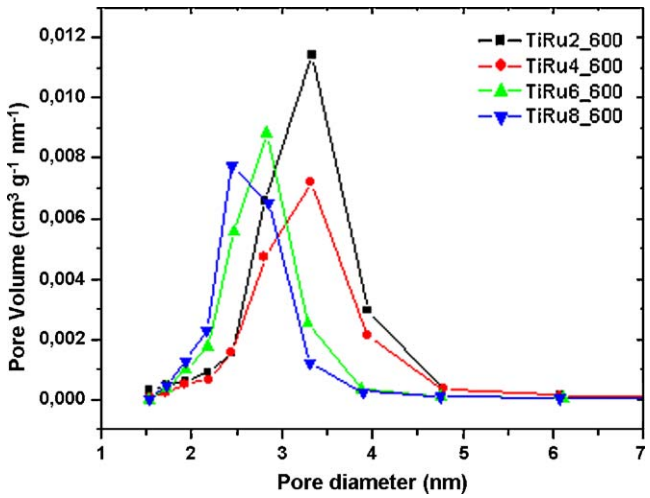

Fig. 3. Pore size distributions of doped titania samples (BJH method).

3.2. Surface area and porosity

Table 2 shows the surface area (BET), the pore radius and total volume of pores related to the mass (porosity) of samples with various contents of RuO_2. All prepared samples displayed a type I isotherm with a desorption hysteresis loop A [32]. The nature of hysteresis is due principally to cylindrical pores open at both ends. The results show that specific surface areas of titania samples have tendency to grow with increasing content of RuO_2. Also, the pore radius and total pore volume of samples increase with increasing content of RuO_2 which is caused by the inclusion of Ru ions in the TiO_2 lattice.

The pore distribution calculated from the BHJ method (see Fig. 3) confirms that Ru-doped titania samples are microporous with pore sizes in the range from 2 nm to 4 nm.

3.3. Scanning electron microscopy (SEM) and high resolution transmission electron microscopy (HRTEM)

It is apparent that the product of homogeneous precipitation of urea and titanium oxo-sulphate consists of approximately spherical round particles; agglomerates of diameter ca. 1 μm to 2 μm. Fig. 4 shows a representative SEM micrograph of doped

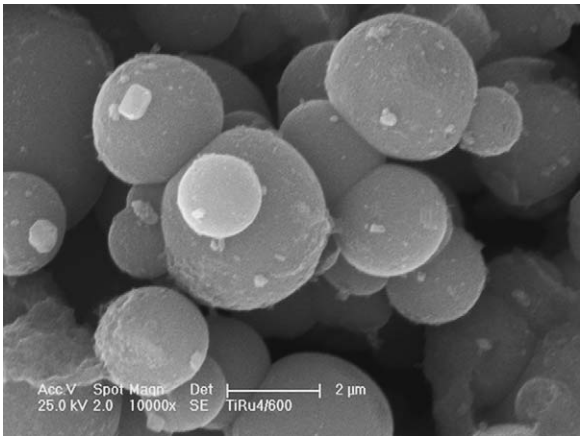

Fig. 4. SEM of TiRu4_600.

Table 2
Characteristics of prepared titania samples doped by variable amounts of $RuCl_3$.

Sample	$RuCl_3$ [g]	Ru content [mol.‰]	Anatase by XRD [%]	RuO_2 by XRD [%]	Anatase crystal. size [nm]	Surface area BET [m^2g^{-1}]	Pore radius [nm]	Total pore volume [$cm^3\ g^{-1}$]
TiRu2_600	0.75	2.878	99.23	0.77	28.4	82.12	33.35	0.134
TiRu3_600	0.5	1.920	99.61	0.39	35.5	50.11	33.07	0.099
TiRu4_600	0.25	0.961	99.37	0.63	36.4	55.29	33.22	0.090
TiRu5_600	0.1	0.385	99.39	0.61	38.8	62.15	21.77	0.075
TiRu6_600	0.05	0.192	99.93	0.07	39.3	50.99	28.32	0.080
TiRu7_600	0.01	0.038	100	0.01	39.5	54.13	24.61	0.071
TiRu8_600	0.005	0.019	100	–*	35.4	57.28	24.51	0.077

*XRD cannot assign such small amount of RuO_2.

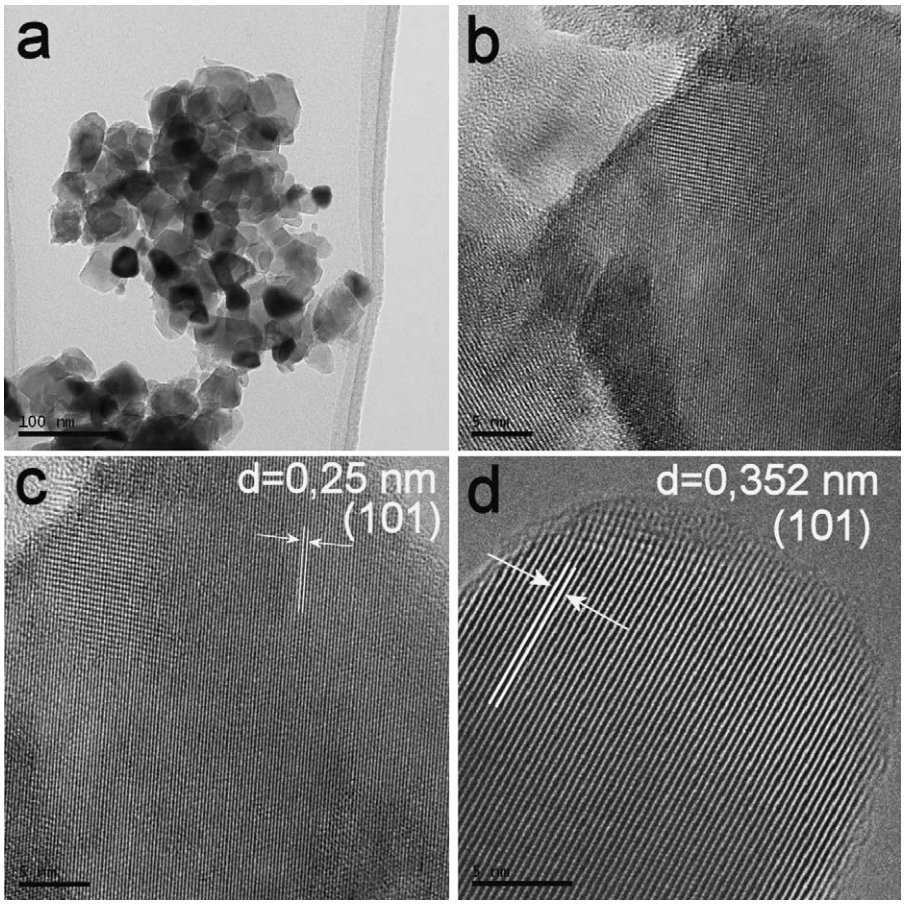

Fig. 5. HRTEM micrographs of (a), (b) TiRu3_600, (c) RuO_2 phase, (d) anatase phase.

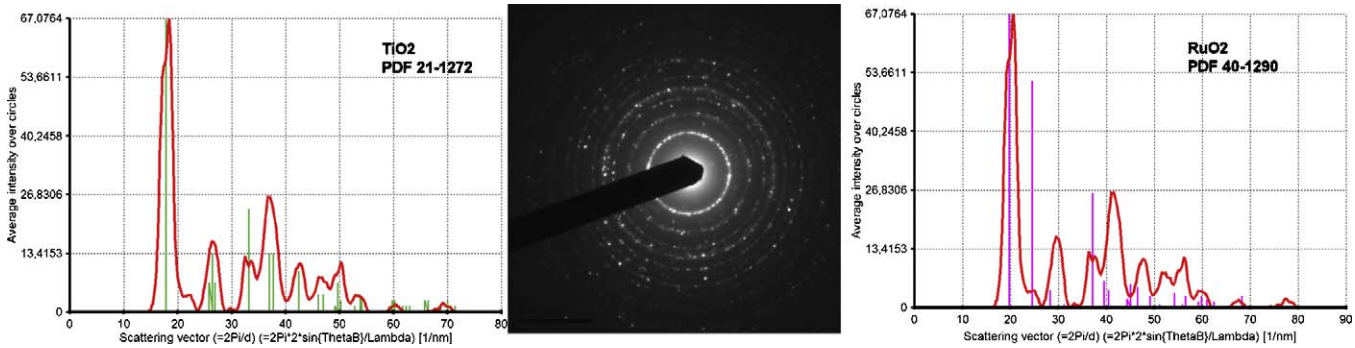

Fig. 6. Electron diffraction pattern of TiRu3_600.

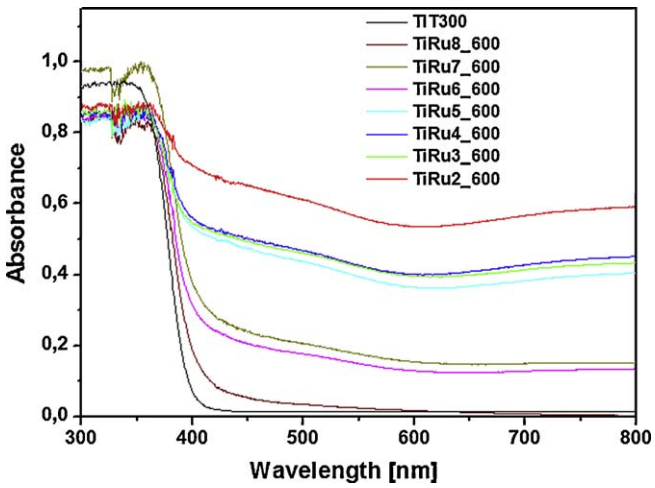

Fig. 7. Absorbance UV/VIS spectra of prepared Ru-doped titania samples and undoped titania (TIT 300).

titania particles. SEM did not illustrate any significant difference between morphological features of doped and undoped particles.

Image processing analysis of HRTEM micrograph is a useful method for refining microstructures in the sense that we can analyze grain sizes and grain boundaries more accurately. Furthermore, from Fourier transform (FFT) spectroscopy it is possible to determine and to index crystallographic planes and find orientations of nanoparticles. Fig. 5 shows HRTEM micrograph of the TiRu3_600 sample. It follows from archived database values (PDF 21-1272, JCPDS PDF2, 2001) that the lattice spacing 0.352 nm (Fig. 5d) corresponds to the [1 0 1] diffraction line of anatase and (PDF 40-1290, JCPDS PDF2, 2001) the lattice spacing 0.25 nm (Fig. 5c) corresponds to the [1 0 1] diffraction line of ruthenium oxide.

Selected areas of the SAED electron diffraction patterns confirm the presence of anatase and RuO_2 phases (see Fig. 6).

3.4. UV/VIS spectra and band-gap energy

The method of UV/VIS diffuse reflectance spectroscopy was employed to estimate the band-gap energies of the prepared Ru-doped titania samples. Firstly, to establish the type of band-to-band transition in these synthesized particles, the absorption data were fitted to equations for direct band-gap transitions. The minimum wavelength required to promote an electron depends upon the band-gap energy E_{bg} of the photocatalyst and is given by:

$$E_{bg}\,[\mathrm{eV}] = 1240\,\lambda^{-1} \quad (1)$$

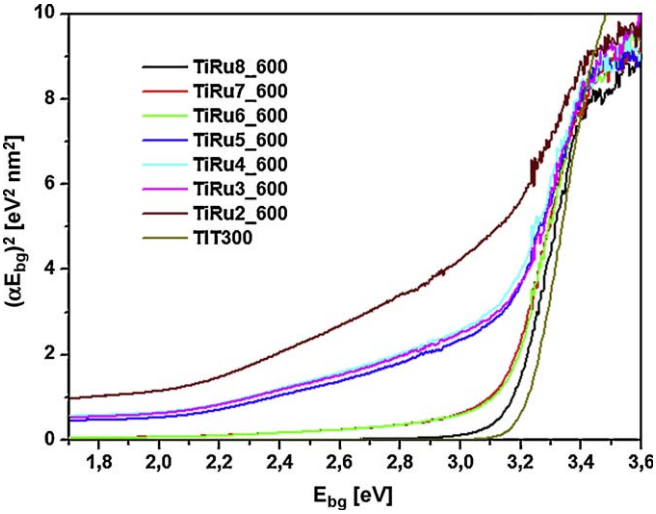

Fig. 8. Band-gap energy of Ru-doped titania samples and undoped titania (TIT 300).

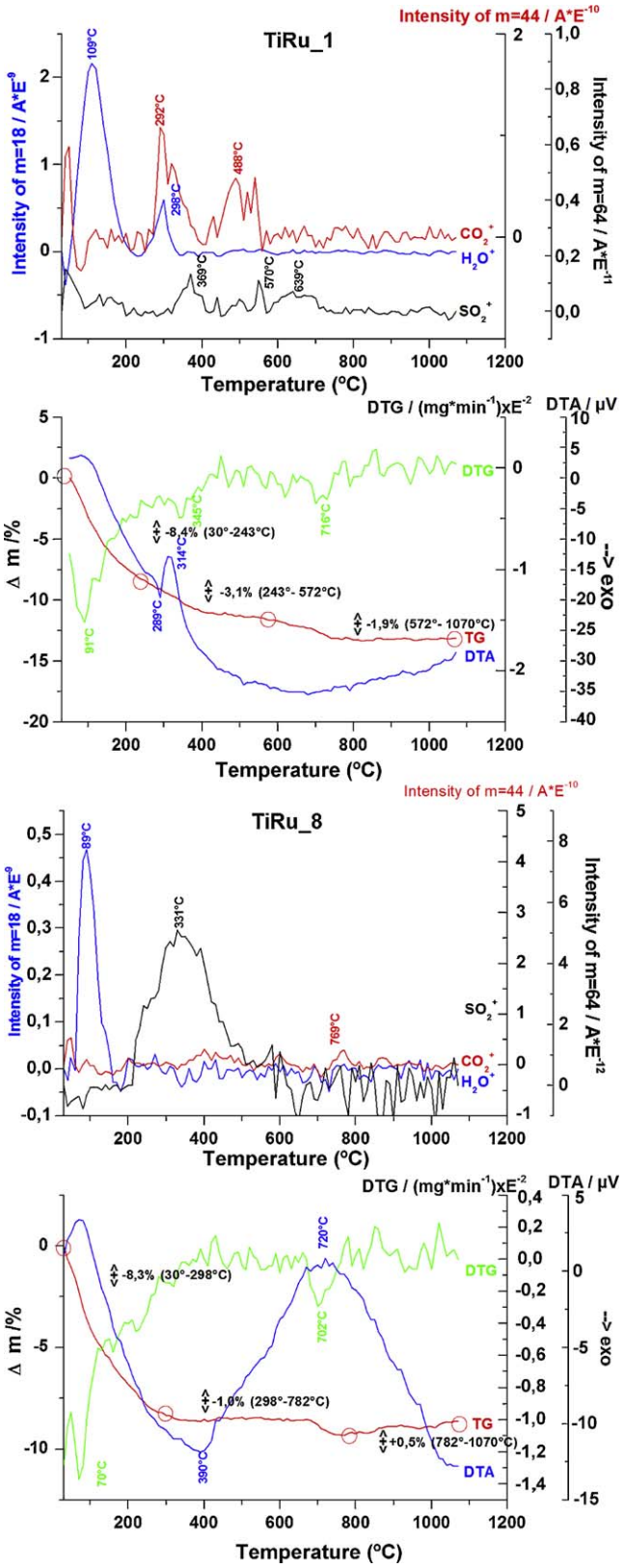

Fig. 9. TGA-DTA curves for titania samples TiRu1 and TiRu8.

Table 3
Rate constant of decomposition of acetone in the gaseous phase.

Sample	Band-gap energy [eV]	Rate constant at 365 nm [min^{-1}]	Amount of CO_2 at 365 nm [%]	Rate constant at 400 nm [min^{-1}]	Amount of CO_2 at 400 nm [%]
TiRu2_600	2.7	0.00038	0.15	0.00034	0.03
TiRu3_600	2.9	0.00033	0.29	0.00034	0.06
TiRu4_600	2.9	0.00041	1.03	0.00032	0.08
TiRu5_600	2.9	0.00045	1.03	0.00054	0.08
TiRu6_600	3.1	0.00059	2.07	0.00058	0.06
TiRu7_600	3.1	0.00058	0.05	0.00057	0.05
TiRu8_600	3.15	0.00050	0.08	0.00042	0.05
TIT 300	3.2	0.0086	3.86	0.00037	0.06
Degussa P25	3.2	0.00041	0.19	–	–

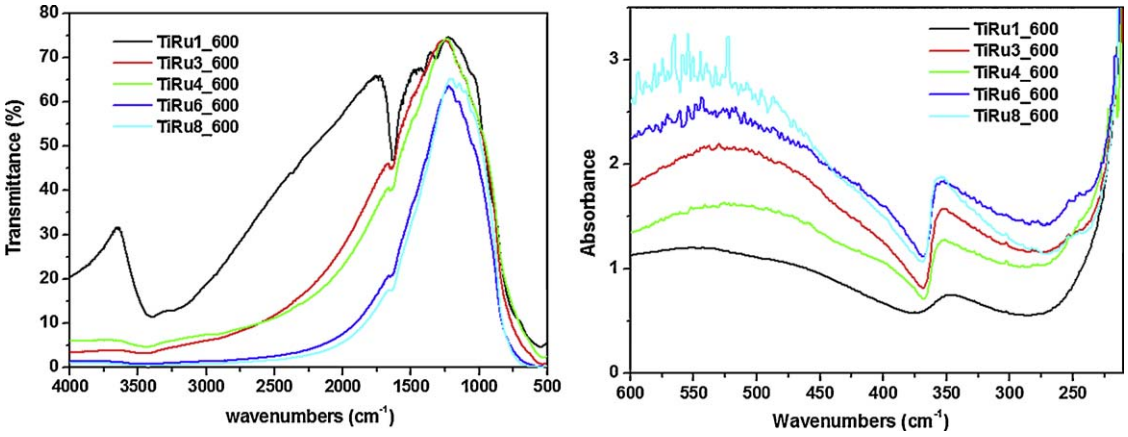

Fig. 10. FT-IR spectra of Ru doped titania samples.

where λ is the wavelength in nanometers [33]. The intensity of the absorbance in the visible region increases with the concentration of the doped Ru ion (see Fig. 7). An obvious red-shift of the absorption edge in VIS absorption spectra is observed and increases with increasing content of RuO_2.

Fig. 8 shows the $(\alpha E_{bg})^2$ versus E_{bg} for an indirect bandgap transition, where α is the absorption coefficient and E_{bg} is the photon energy. The value of E_{bg} extrapolated to $\alpha = 0$ gives an absorption energy, which corresponds to a band-gap energy. The value of 3.20 eV for sample denoted as TIT 300 is reported in the literature for pure anatase nanoparticles [34]. The band-gap energy is also dependent on the extent of doping and decrease with increasing content of RuO_2 (see Table 3).

3.5. Thermogravimetric and differential thermal analysis

The Ru doped samples were studied up to 1200 °C by simultaneous thermogravimetric and differential thermal analysis (TG/DTA). As representative samples were chosen TG/DTA analysis of sample with more (TiRu1) and less (TiRu8) Ru dopant (see Fig. 9). Below 200 °C, the weight loss is considered to be due to the evaporation of water. A significant difference between these two samples is in the exothermic peak of the anatase-rutile transition. Sample TiRu1 has this at 314 °C, while in TiRu8 it is at 720 °C. These results suggest that the temperature of the anatase-rutile transition is dependent on the RuO_2 content.

3.6. Infrared spectroscopy (IR)

Fig. 10 shows the IR spectrum (Transmittance and Absorbance) of Ru doped titania samples after the thermal treatment at 600 °C. The broad absorption peaks at 3400 cm^{-1} and 1626 cm^{-1} correspond to absorbed surface water and hydroxyl groups [35]. These bands, present in all spectra, become weak with decreased RuO_2 content. Weak bands at 1407 cm^{-1} and 1310 cm^{-1} which occur in spectra of sample TiRu1 (sample with the highest content of RuO_2), are assigned to carbonates on sample surfaces resulting from absorption of atmospheric CO_2 [36] and also from absorption of CO_2 released from urea while homogeneous hydrolysis take place. It is obvious that these carbonates are binding by the ruthenium oxide.

3.7. Photocatalytic activity

The photocatalytic activity of as prepared samples was determined by degradation of acetone in the gaseous phase. The photocatalytic activities of samples TiRu2_600 to TiRu8_600 are shown in Table 3. The photocatalytic activities under visible light are strongly affected by the decreased band-gap energy of Ru-doped samples and achieved better activity than non-doped sample TIT 300 and commercial TiO_2 (Degussa P25) which showed no photocatalytic activity under visible light. The rate constant *k*, of the decomposition of acetone under visible light is highest for the sample with 0.07% RuO_2 (TiRu6_600) and with 0.01% RuO_2 (TiRu7_600), both of which have a decreased band-gap energy of 3.1 eV. From measured data is obvious that acetone conversion to CO_2 is decreased by Ru doping.

Under UV light showed better photocatalytic activity non-doped sample TIT 300. Furthermore, sample TiRu6_600 demonstrated good acetone conversion to CO_2 under UV light (see Table 3). These results are in agreement with the red-shift in the absorbance spectra and with the diminished band-gap energy.

4. Conclusions

This paper describes the synthesis of TiO_2 containing varying amounts of ruthenium oxide by homogeneous hydrolysis in the presence of urea.

Ruthenium oxide causes the anatase to rutile transformation for ruthenium doped titania to occur at lower temperatures with increased ruthenium doping.

Doping with Ru ions is accompanied by an improvement in photocatalytic activity using visible light. Samples with added RuO_2 showed visible light activation; the best photocatalytic decomposition of acetone was achieved with the samples TiRu6_600 (0.07% RuO_2 content) and TiRu7_600 (0.01% RuO_2 content).

Acknowledgements

The work was supported by the Academy of Sciences of the Czech Republic (project no. AV0Z40320502) and GAČR (project no. 203 334).

References

[1] A. Fujishima, T.N. Rao, D.A. Tryk, J. Photochem. Photobiol. C: Photochem. Rev. 1 (2000) 1–21.
[2] J.-M. Herrmann, J. Disdier, P. Pichat, S. Malato, J. Blanco, Appl. Catal. B: Environ. 17 (1998) 15–23.
[3] P.V. Kamat, Chem. Rev. 93 (1993) 267–300.
[4] M.R. Hoffmann, S.T. Martin, W. Choi, D.W. Bahnemann, Chem. Rev. 95 (1995) 69–96.
[5] J. Bard, J. Phys. Chem. 86 (1982) 172–177.
[6] M.A. Fox, M.T. Dulay, Chem. Rev. 93 (1993) 341–357.
[7] K. Kato, A. Tsuzuki, H. Taoda, Y. Torii, T. Kato, Y. Butsugan, J. Mater. Sci. 29 (1994) 5911–5915.
[8] R.R. Bacsa, J. Kiwi, Appl. Catal. B Environ. 16 (1998) 19–29.
[9] V. Štengl, J. Šubrt, P. Bezdička, M. Maříková, S. Bakardjieva, Solid State Phen. V 90–91 (2003) 121–126.
[10] M.K. Seery, R. George, P. Floris, S.C. Pillai, J. Photochem. Photobiol. A: Chem. 189 (2007) 258–263.
[11] S.-Z. Chu, S. Inoue, K. Wada, D. Li, J. Suzuki, Langmuir 21 (2005) 8035–8041.
[12] L. Korosi, S. Papp, J. Menesi, V. Zoellmer, A. Richard, I. Dekany, Colloids Surf. A: Physicochem., Eng. Aspects 319 (2008) 136–142.
[13] L. Korosi, I. Dekany, Colloids Surf. A: Physicochem., Eng. Aspects 280 (2006) 146–154.
[14] L. Korosi, A. Oszko, G. Galbacs, A. Richardt, V. Zollmer, I. Dekany, J. Appl. Catal. B 77 (2007) 175–183.
[15] T. Ohno, F. Tanigawa, K. Fujihara, S. Izumi, M. Matsumura, J. Photochem. Photobiol. A: Chem. 127 (1999) 107–110.
[16] K. Kameyama, S. Shohji, S. Onoue, K. Nishimura, K. Yahikozawa, Y. Takasu, J. Electrochem. Soc. 140 (1993) 1034–1037.
[17] K.-H. Chang, C.C. Hu, Electrochim. Acta 52 (2006) 1749–1757.
[18] L.L. Chen, D. Guay, A. Lasia, J. Electrochem. Soc. 143 (1996) 3576–3584.
[19] N. Spataru, J.G. LeHelloco, R. Durand, J. Appl. Electrochem. 26 (1996) 397–402.
[20] O. Simond, C. Comninellis, Electrochim. Acta 42 (1997) 2013–2018.
[21] F. Pico, J. Ibanez, T.A. Centeno, C. Pecharroman, R.M. Rojas, J.M. Amarilla, J.M. Rojo, Electrochim. Acta 51 (2006) 4693–4700.
[22] M. Ocana, M.P. Morales, C.J. Serna, J. Colloid Interface Sci. 212 (1998) 317–323.
[23] K.Ch. Song, Y. Kang, Mater. Lett. 42 (2000) 283–289.
[24] JCPDS PDF-2 release 2001, ICDD Newtown Square, PA, USA.
[25] ICSD Database FIZ Karlsruhe, Germany, 2008.
[26] S. Brunauer, P.H. Emmett, E. Teller, J. Am. Chem. Soc. 60 (1938) 309–319.
[27] E.P. Barret, L.G. Joyner, P.P. Halenda, J. Am. Chem. Soc. 73 (1951) 373–380.
[28] Z.C. Orel, M.K. Gunde, B. Orel, Prog. Org. Coat. 30 (1997) 59–66.
[29] G. Sankar, K.R. Kajman, C.N.R. Rao, Catal. Lett. 8 (1991) 27–36.
[30] Y. Li, Y. Fan, H. Yang, B. Xu, L. Feng, M. Yang, Y. Chen, Chem. Phys. Lett. 372 (2003) 160–165.
[31] S. Bakardjieva, J. Šubrt, V. Štengl, M.J. Dianez, M.J. Sayagues, Appl. Catal. B: Environ. 58 (2005) 193–202.
[32] S. Lowell, J.E. Shields, Powder Surface Area and Porosity, Chapman & Hall, London, 1998.
[33] K.M. Reddy, S.V. Panorama, A.R. Reddy, Mater. Chem. Phys. 78 (2002) 239–245.
[34] D.S. Bhatkhande, V.G. Pangarkar, A.A. Beenackers, J. Chem. Technol. Biotechnol. 77 (2001) 102–116.
[35] G. Shao, X. Zhang, Y. Zhong, Appl. Catal. B: Environ. 82 (2008) 208–218.
[36] P.A. Connor, K.D. Dobson, A.J. McQuillan, Langmuir 15 (1999) 2402–2408.